ISSN 0915-6337

NATIONAL INSTITUTE FOR FUSION SCIENCE

High-η Helicity-induced Shear Alfvén Eigenmodes

N. Nakajima, C.Z. Cheng and M. Okamoto

(Received – Apr. 23, 1992)

NIFS-148 May 1992

RESEARCH REPORT
NIFS Series

This report was prepared as a preprint of work performed as a collaboration research of the National Institute for Fusion Science (NIFS) of Japan. This document is intended for information only and for future publication in a journal after some rearrangements of its contents.

Inquiries about copyright and reproduction should be addressed to the Research Information Center, National Institute for Fusion Science, Nagoya 464-01, Japan.

NAGOYA, JAPAN

High-n helicity-induced shear Alfvén eigenmodes

N.Nakajima, C.Z.Cheng,[1] and M.Okamoto

National Institute for Fusion Science, Nagoya 464-01, Japan

ABSTRACT

The high-n Helicity-induced shear Alfvén Eigenmodes (HAE) are considered both analytically and numerically for the straight helical magnetic system, where n is the toroidal mode number. The eigenmode equation for the high-n HAE modes is derived along the field line and with the aid of the averaging method is shown to reduce to the Mathieu equation asymptotically. The discrete HAE modes are shown to exist inside the continuum spectrum gaps. The continuous spectrum gaps appear around $\omega^2 = \omega_A^2[N(l\iota - m)/2]^2$ for $N = 1, 2, \cdots$, where ω_A is the toroidal Alfvén transit frequency, and l, m, and ι are the polarity of helical coils, the toroidal pitch number of helical coils, and the rotational transform, respectively. For the same ω_A and ι, the frequency of the helical continuum gap is larger than that of the continuum gap in tokamak plasmas by $|l - \iota^{-1}m|$. The polarity of helical coils l plays a crucial role in determining the spectrum gaps and the properties of the high-n HAE modes. The spectrum gaps near the magnetic axis are created by the helical ripple with circular flux surfaces for $l = 1, \text{and } \geq 3$ helicals. For $l = 2$ helical systems, the spectrum gaps are created by the ellipticity of the flux surfaces. These analytical results for the continuum gaps and the existence of the high-n HAE modes in the continuum gaps are confirmed numerically for the $l = 2$ case, and we find that the HAE modes exist for mode structures with the even and the odd parities.

Keywords: Helicity-induced shear Alfvén Eigenmodes (HAE), spectrum gap, Alfvén continuum, straight helical

[1]permanent address: Plasma Physics Laboratory, Princeton University, Princeton, New Jersey 08543, USA.

I. INTRODUCTION

The Toroidicity-indeuced shear Alfvén Eigenmodes (TAE) have been discovered for axisymmetric tokamaks[1-3], and the destabilization of the TAE modes by the α-particles which can result in significant α-particle losses in ignited tokamaks has been theoretically predicted.[4-10] In an axisymmetric toroidal plasma, the magnitude of the toroidal magnetic field is nonuniform over a magnetic flux surface. This nonuniformity of the toroidal magnetic field can cause coupling of neighboring poloidal harmonics and results in the breakup of the shear Alfvén continuous spectrum into small bands of the continuous spectra.[11-13] Inside of the spectrum gaps discrete TAE modes exist as stable toroidal shear Alfvén eigenmodes.[1-3]

In non-axisymmetric toroidal plasmas such as the helical devices, not only the toroidicity but also the helical coils can make the magnitude of the magnetic field nonuniform over a magnetic flux surface. Thus, the straight helical plasmas can also cause the breakup of the shear Alfvén continuous spectrum into small bands of the continuous spectra.

In this paper, we study both analytically and numerically the high-n helicity-induced shear Alfvén eigenmodes (HAE) in a low beta straight helical system. An averaged eigenmode equation along the field line for the high-n HAE modes is obtained by using the averaging method and is reduced to the Mathieu equation[14] asymptotically. It suggests that the spectrum gaps appear around $\omega^2 = \omega_A^2[N(l\iota - m)/2]^2$ for $N = 1, 2, \cdots$, where $\omega_A = v_A/R$ is the toroidal Alfvén transit frequency, $v_A = B_0/\sqrt{\rho_m}$ is the Alfvén velocity, ι is the rotational transform, R is the major radius, B_0 is the uniform toroidal field, and ρ_m is the mass density. The frequency of the helical continuum gap is larger than that of the continuum gap in tokamak plasmas by $|l - qm|$ for the same Alfvén transit frequency ω_A and the rotational transform ι, where $q = \iota^{-1}$ is the safety factor. The existence of the discrete HAE modes is numerically demonstrated in the $l = 2$, $m = 10$ straight helical system, where l and m are the number of helical coils and the toroidal pitch number of helical coils, respectively. The number of helical coils l plays a crucial role in determining the spectrum gaps and the properties of the HAE modes. The spectrum gaps near the magnetic axis are created by the helical ripple for $l = 1$, and ≥ 3 helicals with circular

flux surfaces. But for the $l = 2$ helical system, the spectrum gaps are created by the ellipticity of the magnetic flux surfaces. In contrast to the TAE modes, not only the even modes but also the odd modes exist for the $l = 2$ helical system.

The organization of this paper is as follows. In Sec.II, the high-n ideal magnetohydrodynamic (MHD) Wentzel-Kramers-Brillouin (WKB)-ballooning equation is derived for a low-β straight helical system. Section III gives an analytical treatment of the eigenmode equation by employing the averaging method. The results of numerical calculations are shown in Sec.IV. A summary and discussion is given in Sec.V.

II. BASIC EQUATION

Following Cheng et. al.,[1] the high-n ideal MHD WKB-ballooning equation in the low-β limit is given by

$$\vec{B} \cdot \nabla \left\{ \frac{| \nabla\alpha |^2}{B^2} \vec{B} \cdot \nabla\phi \right\} + \frac{| \nabla\alpha |^2}{B^2} \rho_m \omega^2 \phi = 0, \tag{1}$$

where ρ_m is the mass density, $\nabla\alpha$ is related to the magnetic field by

$$\vec{B} = \nabla\psi \times \nabla\alpha, \tag{2}$$

and ψ is the magnetic flux function. $\nabla\alpha$ is given by

$$\nabla\alpha = \frac{\vec{B} \times \nabla\psi}{| \nabla\psi |^2} + \Lambda \nabla\psi, \tag{3}$$

and Λ is obtained by solving the magnetic differential equation[15]

$$\vec{B} \cdot \nabla\Lambda = -\frac{B^2}{| \nabla\psi |^2} \hat{b} \times \hat{\psi} \cdot \nabla \times (\hat{b} \times \hat{\psi}), \tag{4}$$

where $\hat{b} = \vec{B}/B$, and $\hat{\psi} = \nabla\psi/ | \nabla\psi |$. Note that α is an angle-like, multiple-valued function of position, and Λ contributes to the secular behavior of $\nabla\alpha$.

To consider the high-n HAE modes both analytically and numerically, we use the straight helical vacuum magnetic field as a first approximation. This is consistent with the low-β, large aspect ratio approximation. The straight helical vacuum field in cylindrical

geometry (r, θ, z) is given by[16]

$$\begin{aligned} B_r &= lb\frac{dI_l(\rho)}{d\rho}\sin(l\theta - m\zeta), \\ B_\theta &= l^2 b\frac{I_l(\rho)}{\rho}\cos(l\theta - m\zeta), \\ B_\zeta &= B_0 - lbI_l(\rho)\cos(l\theta - m\zeta), \end{aligned} \tag{5}$$

where $\zeta = z/R$, $\rho = mr/R$, R is the major radius, b represents the helical field strength, and I_l is the l-th order modified Bessel function of the first kind. l and m are the polarity of helical coils and the toroidal pitch number of helical coils, respectively. Note that for even m, l coresponds to the number of helical coils. From the helical symmetry of the the magnetic field given by Eq.(5), the magnetic flux function ψ is given by

$$\psi = \frac{B_0 R}{2lm}\{\rho^2 - \frac{2lb}{B_0}\rho\frac{dI_l(\rho)}{d\rho}\cos(l\theta - m\zeta)\}. \tag{6}$$

Solving the equation of the magnetic field line of force with ζ as the independent variable, we obtain $r = r(\zeta), \theta = \theta(\zeta)$, and we have $\vec{B}\cdot\nabla = (B_\zeta/R)\,(d/d\zeta)$. The initial point of the field line calculation (r_0, θ_0, ζ_0) is chosen at the point of the weakest magnetic field strength in the magnetic flux surface and we set $\theta_0 = 0$ and $\zeta_0 = 0$. $\Lambda(\zeta)$ is obtained by integrating Eq.(4) along the field line with $\Lambda(\zeta_0) = 0$. Then Eq.(1) becomes

$$\frac{d^2}{d\zeta^2}\phi + \frac{d}{d\zeta}\ln\beta\cdot\frac{d}{d\zeta}\phi + \Omega^2\left(\frac{B_0}{B_\zeta}\right)^2\phi = 0, \tag{7}$$

where $\Omega = \omega\tau_A$, $\tau_A = R/v_A$, $v_A = B_0/\sqrt{\rho_m}$, and $\beta \equiv B_\zeta \mid \nabla\alpha \mid^2 / B^2$. Because of helical symmetry of the magnetic field given by Eq.(5), the solutions of Eq.(7) can have either even or odd parities with respect to $\zeta = 0$. With the transformation $\varphi = \phi\sqrt{\beta}$, Eq.(7) has the following Schrödinger type of expression:

$$\frac{d^2}{d\zeta^2}\varphi + U(\Omega^2, \zeta)\varphi = 0, \tag{8}$$

where the potential $U(\Omega^2, \zeta)$ is given by

$$U(\Omega^2, \zeta) = \Omega^2\left(\frac{B_0}{B_\zeta}\right)^2 - \left\{\frac{1}{2}\frac{d^2}{d\zeta^2}\ln\beta + \left[\frac{1}{2}\frac{d}{d\zeta}\ln\beta\right]^2\right\}. \tag{9}$$

III. ANALYTICAL TREATMENT

We use the averaging method[17] to obtain the averaged equation of Eq.(8), and the small ordering parameter is b/B_0 ($\ll$ 1). The equations of the magnetic field line of force are given by[17]

$$\rho = \bar{\rho} + \frac{lb}{B_0}\frac{dI_l(\rho)}{d\rho}\cos(l\theta - m\zeta), \tag{10}$$

$$\theta = \bar{\theta} - \frac{l^2 b}{B_0}\frac{I_l(\rho)}{\rho^2}\sin(l\theta - m\zeta). \tag{11}$$

In the above equation, $\bar{\rho}$ is the averaged radius of the magnetic field line and is defined by

$$\bar{\rho}^2 = \frac{2lm\psi}{B_0 R}, \tag{12}$$

and the averaged θ: $\bar{\theta}$ is given by

$$\bar{\theta} = \iota\zeta, \tag{13}$$

where the rotational transform ι has the following form

$$\iota(\bar{\rho}) = \frac{1}{4}\frac{lm}{\bar{\rho}}\frac{d}{d\bar{\rho}}\left\{\frac{1}{\bar{\rho}}\frac{d}{d\bar{\rho}}\varepsilon_h^2\right\}, \tag{14}$$

with the helical ripple given by

$$\varepsilon_h(\bar{\rho}) = \frac{lb}{B_0} I_l(\bar{\rho}). \tag{15}$$

Using Eqs.(10)-(15), we can evaluate the potential $U(\Omega^2, \zeta)$ given by Eq.(9) in terms of the averaged coordinates. With accuracy up to the order of b/B_0,

$$B_\zeta^2 = B^2 = B_0^2\{1 - 2\varepsilon_h\cos[(l\iota - m)\zeta]\}, \tag{16}$$

$$|\nabla\psi|^2 = \frac{B_0^2\bar{\rho}^2}{l^2}\left\{1 - 2\frac{d^2\varepsilon_h}{d\bar{\rho}^2}\cos[(l\iota - m)\zeta]\right\}. \tag{17}$$

Through long calculations, we can show that

$$\Lambda(\bar{\rho}) = \frac{l^2}{B_0\bar{\rho}^2}\left\{\iota s\zeta - \frac{2lm}{l\iota - m}\frac{d}{d\bar{\rho}}\left(\frac{\varepsilon_h}{\bar{\rho}}\right)\sin[(l\iota - m)\zeta]\right\} \tag{18}$$

with accuracy up to the second order in b/B_0, where s is the shear parameter given by $-(\bar{\rho}/\iota)(d\iota/d\bar{\rho})$, and the second harmonics of the order of $(b/B_0)^2$ are neglected. It is clear

from Eq.(18) that the secular term is proportional to the shear parameter s, which can be shown from Eqs.(14) and (15) to be of second order in b/B_0. Thus, accuracy up to the second order in b/B_0 is needed in deriving Eq.(18).

Using Eqs.(16)-(18) and retaining leading order in b/B_0, we obtain the averaged equation given by

$$\frac{d^2}{d\vartheta^2}\varphi + \{a - 2\epsilon\cos(2\vartheta) - F(\vartheta)\}\varphi = 0, \tag{19}$$

where the new variables are given by

$$a = \left(\frac{2\Omega}{l\iota - m}\right)^2, \tag{20}$$

$$\epsilon = 2\frac{d^2\varepsilon_h}{d\bar{\rho}^2} - (a+1)\varepsilon_h, \tag{21}$$

$$\vartheta = \frac{l\iota - m}{2}\zeta, \tag{22}$$

$$F(\vartheta) = \frac{(2(l\iota - m)\iota s)^2}{\left[(l\iota - m)^2 + (2\iota s\vartheta)^2\right]^2} + \left\{\iota s\left[2\frac{d^2\varepsilon_h}{d\bar{\rho}^2} - \varepsilon_h\right] + 2lm\frac{d}{d\bar{\rho}}\left(\frac{\varepsilon_h}{\bar{\rho}}\right)\right\}\frac{8\iota s\vartheta}{(l\iota - m)^2 + (2\iota s\vartheta)^2}\sin(2\vartheta). \tag{23}$$

The averaged equation has the form of the Mathieu equation[8] in the limit of $\iota s\vartheta \gg 1$ because $F(\vartheta)$ tends to 0 with a damped oscillation. For comparison, the eigenmode equation for the high-n TAE mode is given by[1]

$$\frac{d^2}{d\vartheta_T^2}\varphi + \{a_T - 2\epsilon_T\cos(2\vartheta_T) - F_T(\vartheta_T)\}\varphi = 0, \tag{24}$$

where

$$a_T = \left(\frac{2\Omega}{\iota}\right)^2, \tag{25}$$

$$\epsilon_T = -2a_T\varepsilon_t, \tag{26}$$

$$\vartheta_T = \frac{\theta}{2}, \tag{27}$$

$$F_T(\vartheta_T) = \frac{(2s)^2}{[1 + (2s\vartheta_T)^2]^2}. \tag{28}$$

It is understood that Eqs.(24)-(28) can be obtained from Eqs.(19)-(23) by letting $l = 1$, $m = 0$, $\iota\zeta = \theta$, $\varepsilon_h = 2\varepsilon_t$, and by neglecting $2d^2\varepsilon_h/d\bar{\rho}^2 - \varepsilon_h$ in ϵ and the second term in $F(\vartheta)$. Note that the factor 2 in the relation $\varepsilon_h = 2\varepsilon_t$ comes from the difference of

coordinates between a straight cylinder in the helical and a quasi-torus in the tokamak. It is well known that in the large aspect ratio, low-β tokamak with concentric circular flux surfaces the discrete eigenvalues of high-n TAE modes exist in the frequency gaps where the corresponding Mathieu equation has unstable solutions or unbounded solutions (these frequency gaps are called the continuous spectrum gaps). The existence of the TAE modes is due to the function $F_T(\vartheta_T)$ given by Eq.(28), and only the even TAE modes have been shown to exist.[1] Although the function $F(\vartheta)$ given by Eq.(23) for a straight helical plasma has a slightly different form from $F_T(\vartheta_T)$ for the high-n TAE modes, both functions have similar properties that the function $F(\vartheta)$ vanishes as $\epsilon s\vartheta \gg 1$, and Eq.(19) corresponds to the Mathieu equation. Therefore, we expect the discrete HAE modes to exist in the continuum gaps. In this paper, we shall demonstrate the existence of the HAE modes by numerically solving the high-n MHD WKB-ballooning equation, Eq.(7). For $\epsilon \ll 1$ the continuum gaps can be formed near

$$\Omega^2 = \left[\frac{N(l\iota - m)}{2}\right]^2 \quad \text{for } N = 1, 2, \cdots, \tag{29}$$

with the boundaries of the gaps given by (for $N = 1 \sim 3$):[14]

$$\Omega^2_{N=\pm1} = \left[\frac{l\iota - m}{2}\right]^2 \left\{1 \pm 2\left(\frac{d^2\varepsilon_h}{d\bar{\rho}^2} - \varepsilon_h\right)\right\}, \tag{30}$$

$$\Omega^2_{N=\pm2} = \left[l\iota - m\right]^2 \left\{1 + (\frac{2}{3} \pm 1)\left((2\frac{d^2\varepsilon_h}{d\bar{\rho}^2} - 5\varepsilon_h)/4\right)^2\right\}, \tag{31}$$

$$\Omega^2_{N=\pm3} = \left[\frac{3(l\iota - m)}{2}\right]^2 \left\{1 + \left((\frac{d^2\varepsilon_h}{d\bar{\rho}^2} - 2\varepsilon_h)/6\right)^2 \pm 3\left((\frac{d^2\varepsilon_h}{d\bar{\rho}^2} - 5\varepsilon_h)/6\right)^3\right\}. \tag{32}$$

From Eqs.(29-32), we can see that the continuum gaps in a helical system depend on l, m, ι, ε_h, and $(d^2\varepsilon_h/d\bar{\rho}^2)$. It is clear from the definition of Ω that for the same Alfvén transit time τ_A and the rotational transform ι, the center frequency of the continuum gap in a helical system is larger than that in the tokamak by $|l - qm|$, where $q = \iota^{-1}$ is the safety factor and $a_T = N^2$ is used. For a helical device with $l = 2$, $m = 10$, and $\iota = 0.5$, $|l - qm| = 18$.

It should be noted that the polarity of helical coils l plays a crucial role in creating the spectrum gap and determining the properties of HAE. This role is understood by expanding

the l-th order modified Bessel function of the first kind, I_l, near the geometric center. The helical ripple ε_h given by Eq.(15) increases in proportion to $\bar{\rho}^l$. The magnetic flux surfaces given by Eq.(6) comprise a family of off-center circles, of ellipses, and of circles encircling the origin according to $l = 1$, $l = 2$, and $l \geq 3$, respectively.[16] The effects of the magnetic flux surface shapes are reflected in the phase-dependent terms of Eqs.(17) and (18) through $(d^2\varepsilon_h/d\bar{\rho}^2)$ and $d(\varepsilon_h/\bar{\rho})/d\bar{\rho}$. For $l \neq 2$ helicals with circular flux surfaces, the phase-dependent terms disappear near the magnetic axis because $(d^2\varepsilon_h/d\bar{\rho}^2) \simeq ld(\varepsilon_h/\bar{\rho})/d\bar{\rho} \propto (l-1)\bar{\rho}^{l-2}$. However, for the $l = 2$ helical with elliptic flux surfaces, the phase-dependent terms remain finite. Defining the ellipticity e as the ratio of the long axis to the short axis, we have

$$e^2 = \frac{1 + 2\dfrac{d^2\varepsilon_h}{d\bar{\rho}^2}}{1 - 2\dfrac{d^2\varepsilon_h}{d\bar{\rho}^2}} \tag{33}$$

($e = 1$ for $l \neq 2$, and $e \neq 1$ only for $l = 2$). Thus, the gap structures for straight helical devises with $l \neq 2$ are similar to those for the large aspect ratio, low-β tokamaks in the sense that the contribution from the helical ripple, ε_h and $d^2\varepsilon_h/d\bar{\rho}^2$, makes dominant contribution to the spectrum gaps. But for the $l = 2$ straight helical, the ellipticity e gives the dominant contribution through $d^2\varepsilon_h/d\bar{\rho}^2$ ($d^2\varepsilon_h/d\bar{\rho}^2 \simeq ld(\varepsilon_h/\bar{\rho})/d\bar{\rho} \gg \varepsilon_h$), which is finite near the magnetic axis. The situation is similar to that in a straight plasma column with elliptical cross section.[18–19]

In the following we concentrate on the $l = 2$ helical plasmas. For the $l = 2$ straight helical systems, the ellipticity e or $d^2\varepsilon_h/d\bar{\rho}^2$ ($\simeq ld(\varepsilon_h/\bar{\rho})/d\bar{\rho} \gg \varepsilon_h$) significantly affacts the shear dependent sine term in $F(\vartheta)$ given by Eq.(23). Accordingly, as $\iota s\vartheta$ increases, the first term of $F(\vartheta)$ given by Eq.(23) decreases rapidly as $(\iota s\vartheta)^{-4}$ as well as $F_T(\vartheta_T)$. However, the second term of $F(\vartheta)$damps slowly in proportion to $(e^2-1)/(e^2+1)\cdot(\iota s\vartheta)^{-1}\sin(2\vartheta)$. This term is more effective in determining the properties of the HAE modes as the ellipticity e or $d^2\varepsilon_h/d\bar{\rho}^2$ ($\simeq ld(\varepsilon_h/\bar{\rho})/d\bar{\rho} \gg \varepsilon_h$) increases. Therefore, the properties of the high-n HAE modes can be significantly different from those of the high-n TAE modes. This conclusion is confirmed by the numerical calculations presented in Sec. IV.

IV. NUMERICAL CALCULATIONS

We consider the helical magnetic field given by Eq.(5) with $l = 2$, $m = 10$, aspect ratio $R/a = 8$ where a is the minor radius. b/B_0 is chosen to be 0.45 and 0.68. We choose five magnetic flux surfaces indicated by case(1) to case(5) for a helical system with $b/B_0 = 0.45$ (shown in Tab.I) and five magnetic flux surfaces indicated by case(6) to case(10) for a helical system with $b/B_0 = 0.68$ (shown in Tab.II). The former has a moderate ellipticity, and the latter has a large ellipticity. The rotational transform near the magnetic axis of the former is given by $\iota \simeq 0.51$, which corresponds to the LHD case.[20] The initial point of each flux surface calculation r_0 is chosen in the same toroidal plane and corresponds to the point of the weakest magnetic field strength in each magnetic flux surface. The averaged quantities in the analytical treatment and numerically calculated exact iota ι_E and shear s_E are also shown in Tables I and II. It is clear from Tables I and II that the shear increases with the increase of the averaged radius $\bar{r} = \bar{\rho}R/m$. We also note that the magnetic shear computed from the averaging method s is much smaller than exact magnetic shear s_E. This also results from the truncation error in b/B_0.

Figure 1 shows the variation of $\mid \nabla\alpha \mid^2 / \mid \nabla\alpha \mid^2_{\zeta=0}$ along the magnetic field line for case (2) with the initial condition $\Lambda = 0$ at $\zeta = 0$. Λ increases parabolically along ζ with fast oscillations corresponding to the helical ripple period. This behavior supports our averaging procedure. In Fig.2, we show the boundaries of the lowest continuum gap and the lowest discrete eigenfrequencies of the HAE modes for cases (1)-(5) of the helical system with $b/B_0 = 0.45$. The gap boundaries obtained from both the numerical calculations and the analytical treatments are shown. The analytical gap boundaries are calculated from Eq.(30), and the numerical boundaries are obtained by integrating the eigenmode equation, Eq.(7). It should be noted that the continuum gap still exists near the magnetic axis for $l = 2$ helical systems, and the gap width is large because $d^2\varepsilon_h/d\bar{\rho}$ is finite and is dominant over ε_h. Physically, this is because the magnetic flux surfaces are elliptical near the magnetic axis. In the case of tokamaks, the toroidicity ε_t vanishes at the magnetic axis, and the width of the continuum gap is proportional to the minor radius. Furthermore, in contrast to the TAE modes, the HAE mode frequencies for the $l = 2$ helical systems decrease from near

the upper gap boundary toward the lower gap boundary with the increase of the averaged radius, i.e., with the shear. It is noted that although the analytical treatment breaks down for large b/B_0, the analytical estimate of the gap boundaries gives good indication. Similar conclusions can be drawn for the helical system with $b/B_0 = 0.68$ as shown in Fig. 3. The analytical estimates of the gap boundaries become worse at smaller $\bar{\rho}$ for the larger b/B_0 case shown in Fig.3 than those for the smaller b/B_0 case shown in Fig. 2 due to the breakdown of the expansion in b/B_0. It should be noted that in contrast to the high-n TAE modes, the HAE eigenmodes with odd parity also exist. Figure 4 shows the even eigenfunctions of the HAE modes with corresponding eigenfrequencies in the lowest gap for cases (1)-(5). It is found that the eigenfunctions spread out more along the magnetic field line as the shear decreases. Note that the HAE mode eigenfrequency increases as the magnetic shear decreases. This is opposite to the properties of the TAE modes in tokamaks, where Ω^2 approaches the lower boundary as the shear decreases. Comparing Fig.4 with Fig.1, we see that the eigenfunctions have oscillations with roughly one half period as the helical ripples. Similar features are observed for odd parity HAE modes. Figure 5 shows the odd eigenfunctions of the HAE modes with corresponding eigenfrequencies in the lowest gap for cases (1)-(5). We have also found discrete HAE modes in the higher continuum gaps. Figure 6 shows the eigenfunctions and corresponding eigenfrequencies of an even and an odd HAE mode in the second continuum gap for case (2). Since the fast oscillation of the eigenfunction $\sim e^{i\Omega\zeta}$, the frequency of the oscillation is proportional to the eigenfrequency or the period is inversely proportional to the eigenfrequency.

V. CONCLUSION AND DISCUSSION

The high-n Helicity-induced shear Alfvén Eigenmodes (HAE) are considered both analytically and numerically for a low beta straight helical system, where n is the toroidal mode number. An averaged eigenmode equation for the high-n HAE modes is obtained by using the averaging method. The eigenmode equation reduces to the Mathieu equation asymptotically which suggests the existence of the continuum gaps. The continuous spectrum gaps appear around $\omega^2 = \omega_A^2[N(l\iota - m)/2]^2$ for $N = 1, 2, \cdots$, where $\omega_A = v_A/R$ is

the toroidal Alfvén transit frequency, $v_A = B_0/\sqrt{\rho_m}$ is the Alfvén velocity with the major radius R, the uniform toroidal field B_0, and the mass density ρ_m, and l, m, and ι are the polarity of helical coils, the toroidal pitch number of helical coils, and the rotational transform, respectively. For the same Alfvén transit frequency ω_A and the rotational transform ι, the frequency of the helical continuum gap is larger than that of the toroidal continuum gap by $|l - qm|$, where $q = \iota^{-1}$ is the safety factor. It is found that the polarity of helical coils l plays a crucial role through the shape of the magnetic flux surfaces in determining the spectrum gaps and the properties of the high-n HAE modes. The shape of the magnetic flux surfaces near the magnetic axis is approximately circular for $l = 1, \geq 3$, and elliptic for $l = 2$. Consequently, the spectrum gaps are dominantly created by the helical ripple ε_h for $l \neq 2$. However, for $l = 2$ the continuum gaps are mainly determined by the ellipticity of the flux surfaces e or $d^2\varepsilon_h/d\bar{\rho}^2$ ($\gg \varepsilon_h$). For $l = 2$ case, these analytical results and the existence of the discrete high-n HAE modes in the continuum gaps are confirmed numerically. In contrast to the tokamak case, not only the even modes but also the odd modes exist in each spectrum gap. This is attributed to the slowly decaying oscillatory pert of potential given by the second term of $F(\vartheta)$ (Eq.(23)). This term becomes dominant asymptotically due to the ellipticity e or $d^2\varepsilon_h/d\bar{\rho}^2$ ($\gg \varepsilon_h$) in the $l = 2$ helical system. The spreading of the HAE eigenfunctions along the magnetic field line increases as the shear decreases. In each spectrum gap, many even and odd modes exist and the eigenfunctions spread more and more along the magnetic field line for larger eigenvalues.

In toroidal helical devises, the toroidicity ε_t is also present, and the shaping of the magnetic flux surfaces are easily done by the poloidal coil systems. Since the period of the toroidal field modulation is much slower than the period of the helical field modulation, the continuum gaps due to the toroidal field will be separated from those due to the helical field. For $l = 2$ toroidal helical systems such as CHS[21], Heliotron-E[22], ATF[23], and LHD[20], it is expected that the properties of the helical spectrum gaps and the corresponding HAE modes do not change much from the straight helical case if the ellipticity of the magnetic flux surfaces due to $l = 2$ modes is dominant over the contributions from the helical ripples of other modes with $l \neq 2$. In addition to the HAE modes, we also expect the existence of the TAE modes in the toroidal continuum gap resulting from the variation of

the toroidal field over the magnetic flux surface. More detail examination is now being carried out both analytically and numerically.

ACKNOWLEDGMENTS

The work is supported by the Grant-in-Aid program from the Ministry of Education, Science and Culture. Dr. C.Z.Cheng is supported by the U.S. Department of Energy under Contract DE-AC02-76-CHO-3073. This work was initiated while Dr. C.Z.Cheng visited the National Institute for Fusion Science under the US-Japan Joint Institute for Fusion Theory exchange program in 1990.

REFERENCES

1 C.Z.Cheng, Liu Chen, and M.S.Chance, Ann.Phys.(NY) **161**, 21 (1985).

2 C.Z.Cheng, and M.S.Chance, Phys.Fluids **29**, 3695 (1986).

3 G.Y.Fu and C.Z.Cheng, Phys. Fluids B **2**, 985 (1990).

4 G.Y.Fu and J.W.Van Dam, Phys.Fluid B **1**, 1949 (1989).

5 C.Z.Cheng, Phys. Fluids B **2**, 1427 (1990).

6 C.Z.Cheng, Fusion Technol. **18**, 443 (1990).

7 J.W.Van Dam, G.Y.Fu, and C.Z.Cheng, Fusion Technol. **18**, 461 (1990).

8 C.Z.Cheng, Phys. Fluids B **3**, 2463 (1991).

9 D.J.Sigmar, C.T.Hsu, R.B.White, and C.Z.Cheng, (private communication).

10 H.L.Berk and B.N.Breizman, Phys.Fluid B **2**, 2246 (1990).

11 C.E.Kieras and J.A.Tataronis, J.Plasma Phys. **28**, 395 (1982).

12 O.P.Pogutse and E.I.Yurchenko, Nucl.Fusion **18**, 1629 (1978).

13 D.A.D'Ippolito and J.P.Goedbloed Plasma Phys. **22**, 1091 (1980).

14 N.W.McLachlan, in *Theory and Application of Mathieu Functions* (Dover Publications, Inc. New York 1946) p10.

15 A.Bhattacharjee, J.E.Sedlak, P.L.Similon, M.N.Rosenbluth, and D.W.Ross, Phys.Fluid **26**, 880 (1983).

16 A.I.Morozov, and L.S.Solov'ev, in *Reviews of Plasma Physics*, edited by M.A.Leontovich (Consultant Bureau, New York, 1965), Vol.2, p.42.

17 A.I.Morozov, and L.S.Solov'ev, in *Reviews of Plasma Physics*, edited by M.A.Leontovich (Consultant Bureau, New York, 1965), Vol.2, p.22.

18 R.L.Dewar, R.C.Grimm, J.L.Johnson, E.A.Frieman, J.M.Greene, and P.H.Rutherford, Phys.Fluids **17**, 930 (1974).

19 M.S.Chance, J.M.Greene, R.C.Grimm, and J.L.Johnson, Nucl.Fusion **17**, 65 (1977).

20 A.Iiyoshi, M.Fujiwara, O.Motojima, N.Ohyabu, and K.Yamazaki, Fusion Tech. **17**, 169 (1990).

21 K.Nishimura, K.Matsuoka, M.Fujiwara, K.Yamazaki, J.Todoroki, T.Kamimura, T.Amano, H.Sanuki, S.Okamura, M.Hosokawa, H.Mamada, S.Tanahashi, S.Kubo, Y.Takita, T.Shoji, O.Kanako, H.Iguchi, and C.Takahashi, Fusion Tech. **17**, 86 (1990).

22 T.Obiki, M.Wakatani, M.Sata, S.Sudo, F.Sana, T.Mutoh, K.Itoh, K.Kondo, M.Nakasuga, K.Hanatani, H.Zushi, T.Mizuuchi, H.Kanako, H.Okada, Y.Takeiri, Y.Nakamura, S.Besshou, Y.Ijiri, M.Iima, T.Senju, K.Yaguchi, T.Baba, S.Kobayashi, K.Matsuo, K.Muraoka, T.Tsukishima, and M.Nakajima, Fusion Tech. **17**, 101 (1990).

23 J.F.Lyon, G.L.Bell, J.D.Bell, R.D.Benson, T.S.Bigelow, K.K.Chipley, R.J.Colchin, M.J.Cole, E.C.Crume, J.L.Dunlap, A.C.England, J.C.Glowienka, R.H.Goulding, J.H.Harris, D.L.Hillis, S.Hirose, L.D.Horton, H.C.Howe, R.C.Isler, T.C.Jernigan, R.L.Johnson, R.A.Langley, M.M.Menon, P.K.Mioduszewski, R.N.Morris, M.Murakami, G.H.Neilson, B.E.Nelson, D.A.Rasmussen, J.A.Rome, M.J.Saltmarsh, P.B.Thompson, M.R.Wade, J.A.White, T.L.White, J.C.Whitson, J.B.Wilgen, and W.R.Wing, Fusion Tech. **17**, 33 (1990).

TABLE I. AVERAGED QUANTITIES FOR MODERATE ELLIPTICITY

case	r_0	$\bar{r}$	ι_E	ι	s_E	s	ε_h	$d^2\varepsilon_h/d\bar{\rho}^2$	e
case(1)	0.250	0.184	0.558	0.520	-0.087	-0.052	0.0060	0.231	1.65
case(2)	0.500	0.361	0.634	0.559	-0.358	-0.195	0.0232	0.248	1.72
case(3)	0.750	0.520	0.782	0.620	-0.891	-0.390	0.0493	0.274	1.85
case(4)	0.900	0.603	0.926	0.663	-1.467	-0.511	0.0671	0.291	1.95
case(5)	0.950	0.628	0.987	0.677	-1.747	-0.549	0.0730	0.298	1.99

TABLE II. AVERAGED QUANTITIES FOR LARGE ELLIPTICITY

case	r_0	$\bar{r}$	t_E	t	s_E	s	ε_h	$d^2\varepsilon_h/d\bar{\rho}^2$	e
case(6)	0.100	0.056	1.344	1.159	-0.016	-0.005	0.0001	0.341	2.30
case(7)	0.250	0.139	1.403	1.174	-0.106	-0.030	0.0051	0.345	2.34
case(8)	0.500	0.262	1.642	1.219	-0.520	-0.105	0.0184	0.358	2.46
case(9)	0.600	0.303	1.810	1.241	-0.896	-0.139	0.0246	0.365	2.52
case(10)	0.800	0.359	2.423	1.276	-4.195	-0.193	0.0348	0.375	2.64

FIGURE CAPTIONS

FIG.1 $| \nabla\alpha |^2 / | \nabla\alpha |^2_{\zeta=0}$ along the magnetic field line for case (2) with the initial condition $\Lambda = 0$ at $\zeta = 0$.

FIG.2 The boundaries of the lowest continuum gap and the lowest discrete eigenfrequencies of the HAE modes for cases (1)-(5) of the helical system with $b/B_0 = 0.45$ as shown in Tab.I. The dotted curves indicate the boundaries obtained from the analytical treatments using Eq.(30). The broken curves designate the boundaries obtained from the numerical calculations. The open circles and crosses show the lowest even and odd eigenfrequencies, respectively.

FIG.3 The boundaries of the lowest continuum gap and the lowest discrete eigenfrequencies of the HAE modes for cases (6)-(10) of the helical system with $b/B_0 = 0.68$ as shown in Tab.II. The symbols are the same as those in Fig.2.

FIG.4 The even eigenfunctions of the HAE modes with corresponding eigenfrequencies in the lowest gap for cases (1)-(5). The period of the oscillation of each eigenfunction is roughly one half of the helical ripple period shown in Fig.1.

FIG.5 The odd eigenfunctions of the HAE modes with corresponding eigenfrequencies in the lowest gap for cases (1)-(5).

FIG.6 The even and odd eigenfunctions of the HAE modes with corresponding eigenfrequencies in the second gap for case (2).

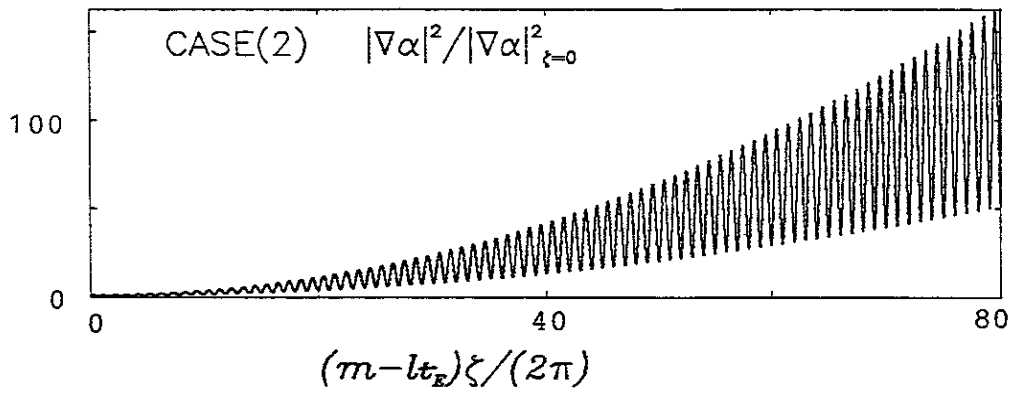

Fig.1 N.Nakajima et al.

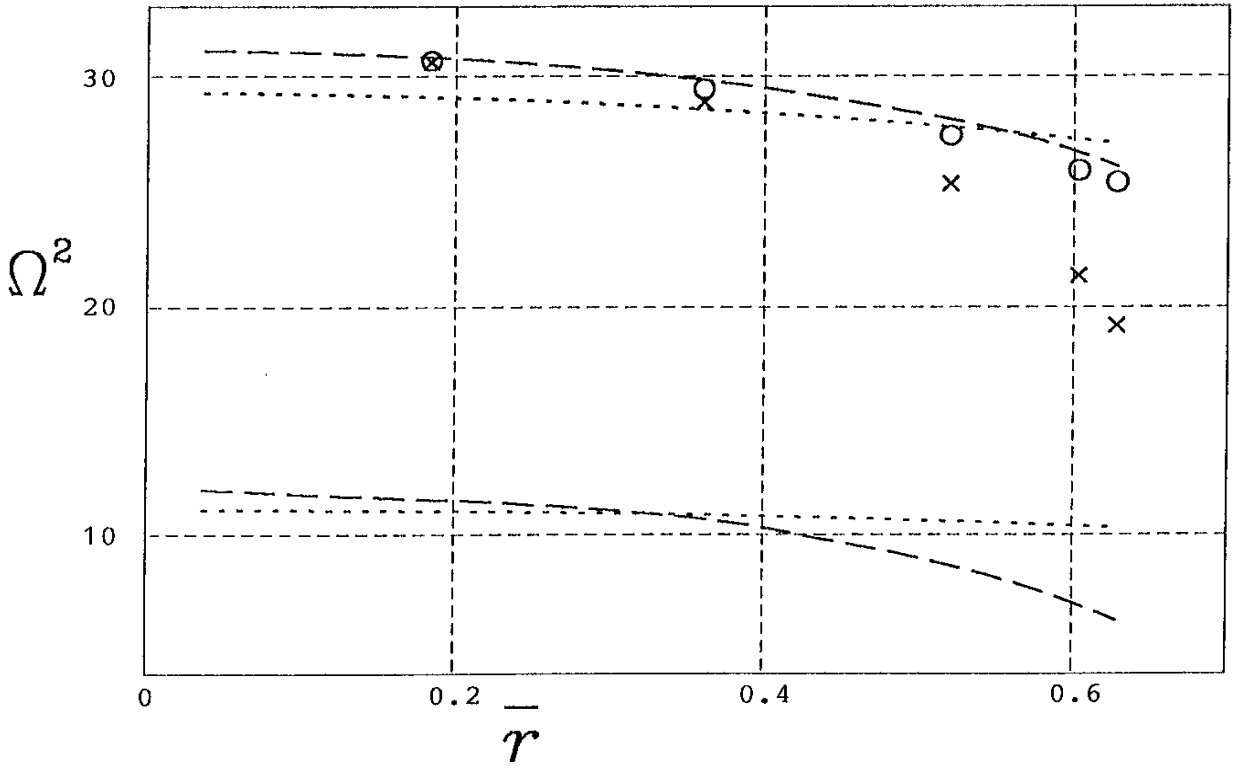

Fig.2 N.Nakajima et al.

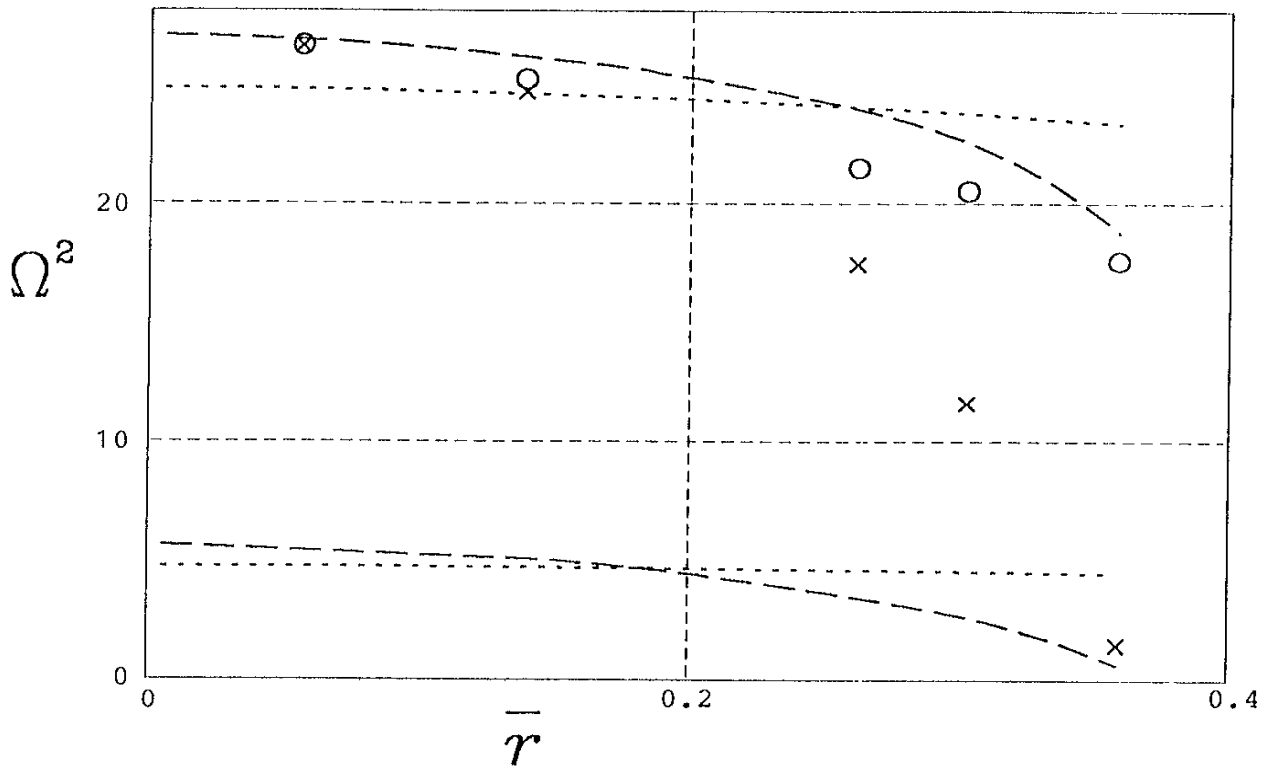

Fig.3 N.Nakajima et al.

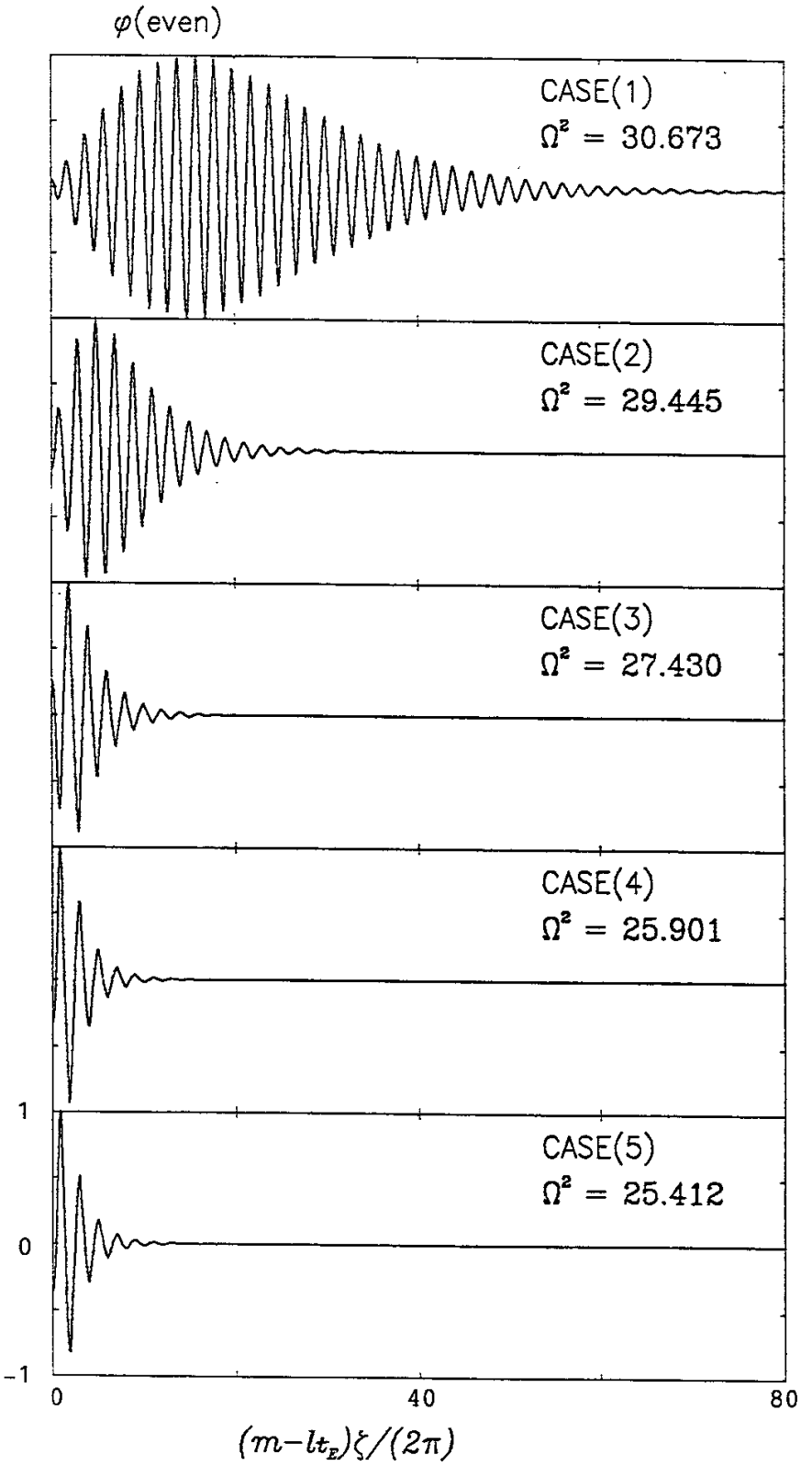

Fig.4 N.Nakajima et al.

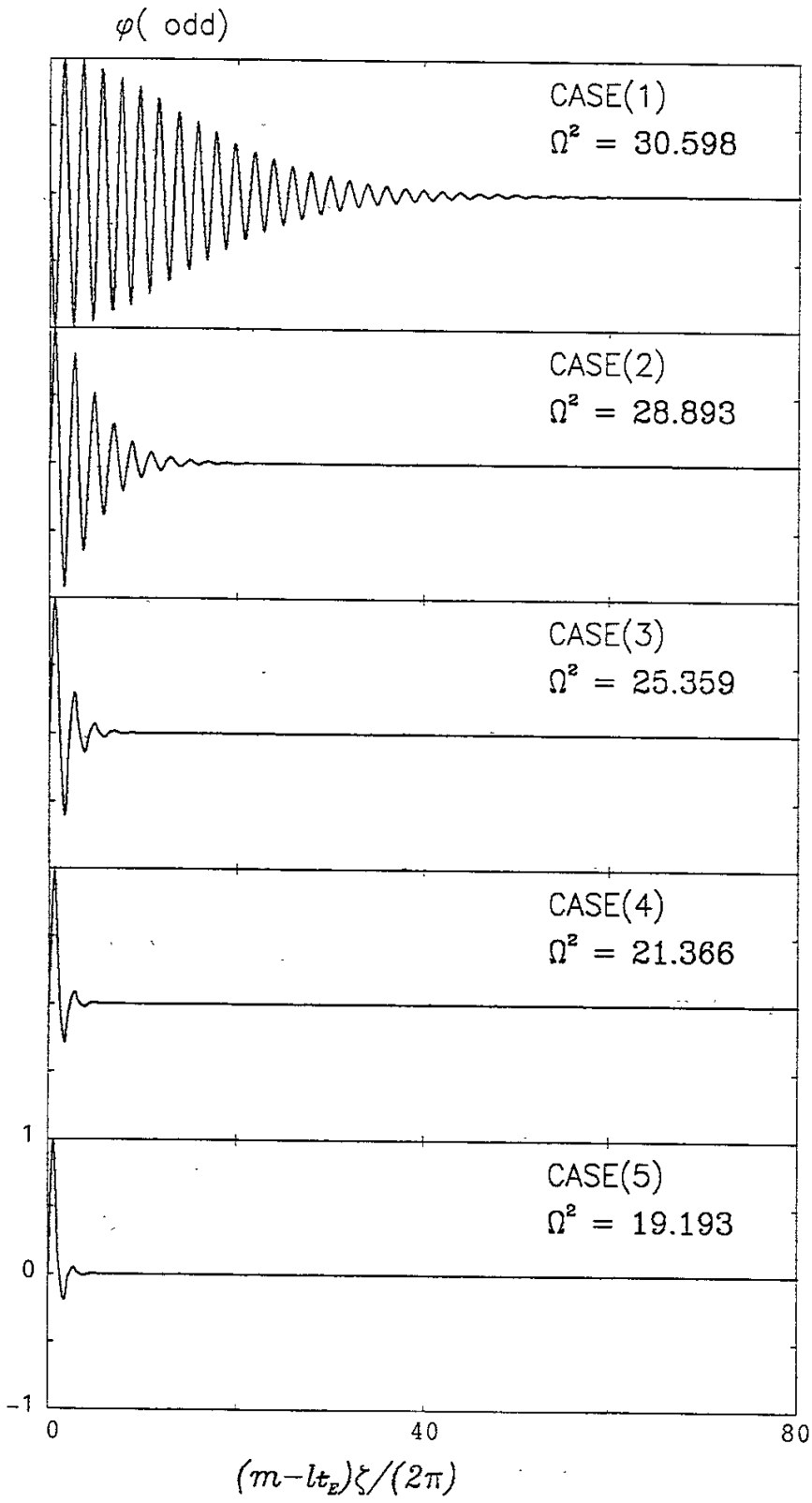

Fig.5 N.Nakajima et al.

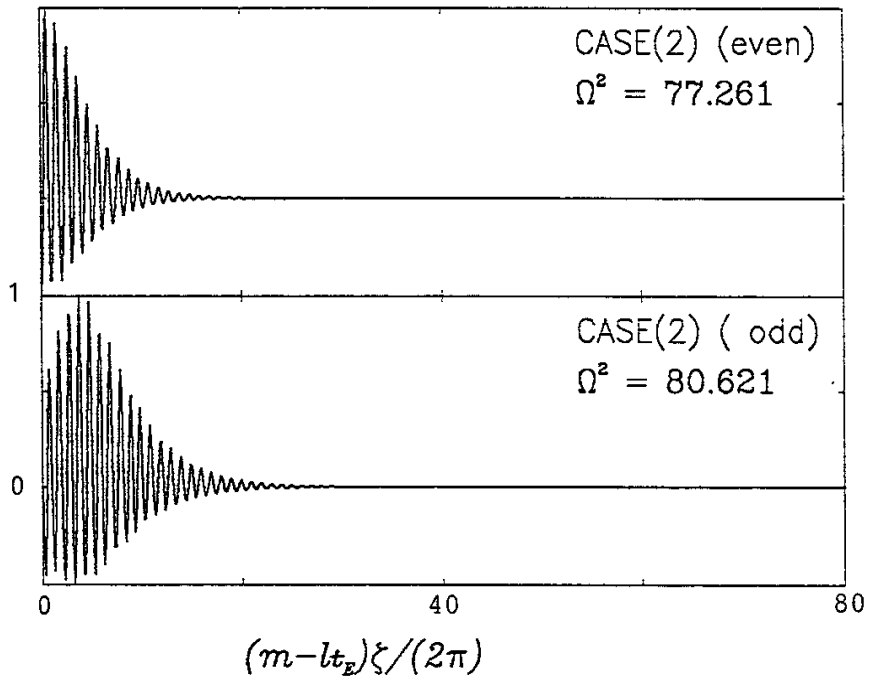

Fig.6 N.Nakajima et al.

Recent Issues of NIFS Series

NIFS-97 K. Itoh, S. - I. Itoh, H. Sanuki, A. Fukuyama, *An H-mode-Like Bifurcation in Core Plasma of Stellarators;* Jun. 1991

NIFS-98 H. Hojo, T. Watanabe, M. Inutake, M. Ichimura and S. Miyoshi, *Axial Pressure Profile Effects on Flute Interchange Stability in the Tandem Mirror GAMMA 10;* Jun. 1991

NIFS-99 A. Usadi, A. Kageyama, K. Watanabe and T. Sato, *A Global Simulation of the Magnetosphere with a Long Tail : Southward and Northward IMF;* Jun. 1991

NIFS-100 H. Hojo, T. Ogawa and M. Kono, *Fluid Description of Ponderomotive Force Compatible with the Kinetic One in a Warm Plasma* ; July 1991

NIFS-101 H. Momota, A. Ishida, Y. Kohzaki, G. H. Miley, S. Ohi, M. Ohnishi K. Yoshikawa, K. Sato, L. C. Steinhauer, Y. Tomita and M. Tuszewski *Conceptual Design of D-^{3}He FRC Reactor "ARTEMIS"* ; July 1991

NIFS-102 N. Nakajima and M. Okamoto, *Rotations of Bulk Ions and Impurities in Non-Axisymmetric Toroidal Systems* ; July 1991

NIFS-103 A. J. Lichtenberg, K. Itoh, S. - I. Itoh and A. Fukuyama, *The Role of Stochasticity in Sawtooth Oscillation* ; Aug. 1991

NIFS-104 K. Yamazaki and T. Amano, *Plasma Transport Simulation Modeling for Helical Confinement Systems;* Aug. 1991

NIFS-105 T. Sato, T. Hayashi, K. Watanabe, R. Horiuchi, M. Tanaka, N. Sawairi and K. Kusano, *Role of Compressibility on Driven Magnetic Reconnection ;* Aug. 1991

NIFS-106 Qian Wen - Jia, Duan Yun - Bo, Wang Rong - Long and H. Narumi, *Electron Impact Excitation of Positive Ions - Partial Wave Approach in Coulomb - Eikonal Approximation* ; Sep. 1991

NIFS-107 S. Murakami and T. Sato, *Macroscale Particle Simulation of Externally Driven Magnetic Reconnection;* Sep. 1991

NIFS-108 Y. Ogawa, T. Amano, N. Nakajima, Y. Ohyabu, K. Yamazaki, S. P. Hirshman, W. I. van Rij and K. C. Shaing, *Neoclassical Transport Analysis in the Banana Regime on Large Helical Device (LHD) with the DKES Code;* Sep. 1991

NIFS-109 Y. Kondoh, *Thought Analysis on Relaxation and General Principle to Find Relaxed State;* Sep. 1991

NIFS-110 H. Yamada, K. Ida, H. Iguchi, K. Hanatani, S. Morita, O. Kaneko, H. C. Howe, S. P. Hirshman, D. K. Lee, H. Arimoto, M. Hosokawa, H. Idei, S. Kubo, K. Matsuoka, K. Nishimura, S. Okamura, Y. Takeiri, Y. Takita and C. Takahashi, *Shafranov Shift in Low-Aspect-Ratio Heliotron / Torsatron CHS* ; Sep 1991

NIFS-111 R. Horiuchi, M. Uchida and T. Sato, *Simulation Study of Stepwise Relaxation in a Spheromak Plasma ;* Oct. 1991

NIFS-112 M. Sasao, Y. Okabe, A. Fujisawa, H. Iguchi, J. Fujita, H. Yamaoka and M. Wada, *Development of Negative Heavy Ion Sources for Plasma Potential Measurement* ; Oct. 1991

NIFS-113 S. Kawata and H. Nakashima, *Tritium Content of a DT Pellet in Inertial Confinement Fusion* ; Oct. 1991

NIFS-114 M. Okamoto, N. Nakajima and H. Sugama, *Plasma Parameter Estimations for the Large Helical Device Based on the Gyro-Reduced Bohm Scaling* ; Oct. 1991

NIFS-115 Y. Okabe, *Study of Au^- Production in a Plasma-Sputter Type Negative Ion Source* ; Oct. 1991

NIFS-116 M. Sakamoto, K. N. Sato, Y. Ogawa, K. Kawahata, S. Hirokura, S. Okajima, K. Adati, Y. Hamada, S. Hidekuma, K. Ida, Y. Kawasumi, M. Kojima, K. Masai, S. Morita, H. Takahashi, Y. Taniguchi, K. Toi and T. Tsuzuki, *Fast Cooling Phenomena with Ice Pellet Injection in the JIPP T-IIU Tokamak;* Oct. 1991

NIFS-117 K. Itoh, H. Sanuki and S. -I. Itoh, *Fast Ion Loss and Radial Electric Field in Wendelstein VII-Λ Stellarator;* Oct. 1991

NIFS-118 Y. Kondoh and Y. Hosaka, *Kernel Optimum Nearly-analytical Discretization (KOND) Method Applied to Parabolic Equations <<KOND-P Scheme>>;* Nov. 1991

NIFS-119 T. Yabe and T. Ishikawa, *Two- and Three-Dimensional Simulation Code for Radiation-Hydrodynamics in ICF;* Nov. 1991

NIFS-120 S. Kawata, M. Shiromoto and T. Teramoto, *Density-Carrying Particle Method for Fluid* ; Nov. 1991

NIFS-121 T. Ishikawa, P. Y. Wang, K. Wakui and T. Yabe, *A Method for the*

High-speed Generation of Random Numbers with Arbitrary Distributions; Nov. 1991

NIFS-122 K. Yamazaki, H. Kaneko, Y. Taniguchi, O. Motojima and LHD Design Group, *Status of LHD Control System Design ; Dec. 1991*

NIFS-123 Y. Kondoh, *Relaxed State of Energy in Incompressible Fluid and Incompressible MHD Fluid* ; Dec. 1991

NIFS-124 K. Ida, S. Hidekuma, M. Kojima, Y. Miura, S. Tsuji, K. Hoshino, M. Mori, N. Suzuki, T. Yamauchi and JFT-2M Group, *Edge Poloidal Rotation Profiles of H-Mode Plasmas in the JFT-2M Tokamak ;* Dec. 1991

NIFS-125 H. Sugama and M. Wakatani, *Statistical Analysis of Anomalous Transport in Resistive Interchange Turbulence* ;Dec. 1991

NIFS-126 K. Narihara, *A Steady State Tokamak Operation by Use of Magnetic Monopoles* ; Dec. 1991

NIFS-127 K. Itoh, S. -I. Itoh and A. Fukuyama, *Energy Transport in the Steady State Plasma Sustained by DC Helicity Current Drive* ;Jan. 1992

NIFS-128 Y. Hamada, Y. Kawasumi, K. Masai, H. Iguchi, A. Fujisawa, JIPP T-IIU Group and Y. Abe, *New Hight Voltage Parallel Plate Analyzer* ; Jan. 1992

NIFS-129 K. Ida and T. Kato, *Line-Emission Cross Sections for the Charge-exchange Reaction between Fully Stripped Carbon and Atomic Hydrogen in Tokamak Plasma*; Jan. 1992

NIFS-130 T. Hayashi, A. Takei and T. Sato, *Magnetic Surface Breaking in 3D MHD Equilibria of l=2 Heliotron* ; Jan. 1992

NIFS-131 K. Itoh, K. Ichiguchi and S. -I. Itoh, *Beta Limit of Resistive Plasma in Torsatron/Heliotron* ; Feb. 1992

NIFS-132 K. Sato and F. Miyawaki, *Formation of Presheath and Current-Free Double Layer in a Two-Electron-Temperature Plasma* ; Feb. 1992

NIFS-133 T. Maruyama and S. Kawata, *Superposed-Laser Electron Acceleration* Feb. 1992

NIFS-134 Y. Miura, F. Okano, N. Suzuki, M. Mori, K. Hoshino, H. Maeda, T. Takizuka, JFT-2M Group, S.-I. Itoh and K. Itoh, *Rapid Change of Hydrogen Neutral Energy Distribution at L/H-Transition in JFT-2M H-mode ;* Feb. 1992

NIFS-135 H. Ji, H. Toyama, A. Fujisawa, S. Shinohara and K. Miyamoto *Fluctuation and Edge Current Sustainment in a Reversed-Field-Pinch;* Feb. 1992

NIFS-136 K. Sato and F. Miyawaki, *Heat Flow of a Two-Electron-Temperature Plasma through the Sheath in the Presence of Electron Emission;* Mar. 1992

NIFS-137 T. Hayashi, U. Schwenn and E. Strumberger, *Field Line Diversion Properties of Finite ß Helias Equilibria;* Mar. 1992

NIFS-138 T. Yamagishi, *Kinetic Approach to Long Wave Length Modes in Rotating Plasmas*; Mar. 1992

NIFS-139 K. Watanabe, N. Nakajima, M. Okamoto, Y. Nakamura and M. Wakatani, *Three-dimensional MHD Equilibrium in the Presence of Bootstrap Current for Large Helical Device (LHD)*; Mar. 1992

NIFS-140 K. Itoh, S. -I. Itoh and A. Fukuyama, *Theory of Anomalous Transport in Toroidal Helical Plasmas;* Mar. 1992

NIFS-141 Y. Kondoh, *Internal Structures of Self-Organized Relaxed States and Self-Similar Decay Phase;* Mar. 1992

NIFS-142 U. Furukane, K. Sato, K. Takiyama and T. Oda, *Recombining Processes in a Cooling Plasma by Mixing of Initially Heated Gas*; Mar. 1992

NIFS-143 Y. Hamada, K. Masai, Y. Kawasumi, H. Iguchi, A. Fijisawa and JIPP T-IIU Group, *New Method of Error Elimination in Potential Profile Measurement of Tokamak Plasmas by High Voltage Heavy Ion Beam Probes;* Apr. 1992

NIFS-144 N. Ohyabu, N. Noda, Hantao Ji, H. Akao, K. Akaishi, T. Ono, H. Kaneko, T. Kawamura, Y. Kubota, S. Morimoto. A. Sagara, T. Watanabe, K. Yamazaki and O. Motojima, *Helical Divertor in the Large Helical Device;* May 1992

NIFS-145 K. Ohkubo and K. Matsumoto, *Coupling to the Lower Hybrid Waves with the Multijunction Grill*; May 1992

NIFS-146 K. Itoh, S. -I.Itoh, A. Fukuyama, S. Tsuji and Allan J. Lichtenberg, *A Model of Major Disruption in Tokamaks*; May 1992

NIFS-147 S. Sasaki, S. Takamura, M. Ueda, H. Iguchi, J. Fujita and K. Kadota, *Edge Plasma Density Reconstruction for Fast Monoenergetic Lithium Beam Probing*; May 1992